Growth of Ultrahigh Density Vertically Aligned Carbon Nanotube Forests for Interconnects

Santiago Esconjauregui,[†] Martin Fouquet,[†] Bernhard C. Bayer,[†] Caterina Ducati,[‡] Rita Smajda,[§] Stephan Hofmann,[†] and John Robertson[†],*

[†]Engineering Department, Cambridge University, Cambridge CB2 1PZ, U.K., [‡]Materials Science Department, Cambridge University, Cambridge CB2 3QZ, U.K., and [§]Laboratory of Complex Mater Physics, Ecole Polytechnique Fédérale de Lausanne, Lausanne CH-1015, Switzerland

Carbon nanotubes (CNTs) have a unique set of properties, such as high current carrying capacity, high thermal conductivity, mechanical strength, and extremely large surface area,[1−8] which allow numerous applications. It is now possible to grow single-walled nanotubes (SWNTs) efficiently, in high purity, in bulk and on surfaces,[9−13] so that the production limitations for many applications appear to be overcome. However, on closer inspection, for many key applications of nanotube forests, existing growth methods produce forests whose area density and performance are still 1−2 orders of magnitude too low.

Consider the example of replacing copper interconnects in integrated circuits by CNTs, a key milestone of the Semiconductor Roadmap.[14−16] CNT interconnects will not be used unless their resistance is lower than that of copper, which requires a CNT area density of at least 2×10^{13} cm^{-2} to lower their series resistance arising from the quantum resistance. However, the highest density of SWNTs achieved so far is only $\sim 7 \times 10^{11}$ cm^{-2},[7,17−21] a factor 30 times too low (Figure 1).

A similar problem occurs for heat spreaders. While the thermal conductivity of a single nanotube may be comparable to that of a solid rod of diamond,[3] if the nanotube forest only fills 3% of the available cross section, the actual thermal conductance is 30 times lower and much less useful.[22,23] To overcome these limits, we need essentially fully dense forests. We present here a catalyst design to grow ultrahigh density nanotube forests, close to the required 2×10^{13} cm^{-2} density, with even higher densities possible.

ABSTRACT We present a general catalyst design to synthesize ultrahigh density, aligned forests of carbon nanotubes by cyclic deposition and annealing of catalyst thin films. This leads to nanotube forests with an area density of at least 10^{13} cm^{-2}, over 1 order of magnitude higher than existing values, and close to the limit of a fully dense forest. The technique consists of cycles of ultrathin metal film deposition, annealing, and immobilization. These ultradense forests are needed to use carbon nanotubes as vias and interconnects in integrated circuits and thermal interface materials. Further density increase to 10^{14} cm^{-2} by reducing nanotube diameter is possible, and it is also applicable to nanowires.

KEYWORDS: carbon nanotubes · growth mechanism · chemical vapor deposition · catalyst design · high density forests · interconnects

SWNT forests are grown by catalytic chemical vapor deposition (CVD), such as in the "super growth" method. The nanotube density is similar to that of catalyst nanoparticles from which they nucleate and grow. The usual catalyst preparation method is to deposit a thin film of catalyst (such as Fe) on an underlying support layer (eg Al oxide) and anneal it, converting the Fe film into many catalytically active nanoparticles. This restructuring is driven by surface energy minimization from Young's equation[24,25] because the oxide surface energy is less than that of the metal. The nanoparticle diameter (d) scales with average thickness of the initial Fe film (h) as $d \sim 6h$[25,26] (Figure 1), so the nanoparticle density N varies as

$$N \sim \frac{1}{30 d^2} \qquad (1)$$

with the prefactor depending on the contact angle of the Fe and support. However, there is a limit to how thin an initial Fe film can be (~ 0.2 nm) without losing it by diffusion into the substrate. This limits the maximum density to $7 \times 10^{11} - 10^{12}$ cm^{-2}. This is the nanotube density found by Futaba[7,17,27]
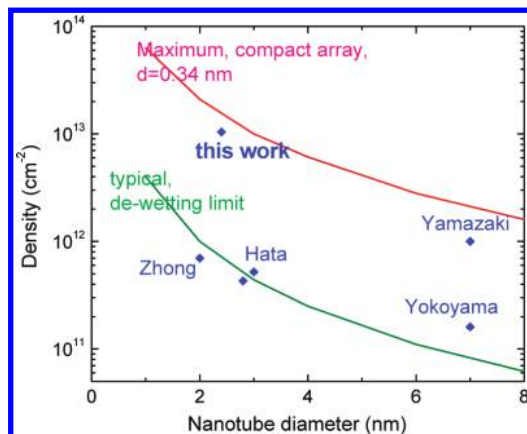
Figure 1. Comparison of maximum and typical nanotube densities *vs* nanotube diameter, including previous and present nanotube densities.[7,16−18,21,27]

and Zhong,[18] much below the theoretical maximum of a fully dense forest (Figure 1).

RESULTS

We now describe how to increase this density to over 10^{13} cm^{-2} by repeated deposition of catalyst layers. Normally, depositing a metal layer twice just makes a thicker layer, which, by eq 1, anneals into a lower particle density. If we deposit a layer, anneal it, and then deposit and anneal a second layer on top of this, it just sinters into the first layer, also giving a lower density. However, if we can restructure each layer *independently*, we can increase density *cumulatively*. We must deposit the first layer, restructure it, temporarily *immobilize* it, deposit the next layer, restructure, immobilize, and so on (Figure 2). If each restructuring cycle is independent, the density increases cumulatively. We can continue the cycles to build up a much higher nanoparticle density.

The key to temporarily immobilizing each nanoparticle layer is to convert it into a less mobile phase, such as an oxide (or nitride). The initial metal film is so thin that it is discontinuous. Annealing converts it to nanoparticles. Intentional or adventitious oxidation then occurs. We then deposit the next discontinuous metal layer and restructure it. This leads to three practical methods to achieve a high nanoparticle density:

(1) Deposit an Fe layer, anneal the metal into droplets, allow it to oxidize, cool. Deposit the next Fe layer, anneal it, oxidize it, and so on. Oxidation can happen by exposure to either air or water vapor in a low vacuum.

(2) Deposit Fe, deposit a 0.2 nm discontinuous Al layer on the Fe, anneal, allow Al to oxidize into discontinuous Al_2O_3 layer, cool, deposit more Fe and Al, anneal, and so on.

(3) Deposit Fe, anneal, plasma oxidize or nitride,[28,29] cool, deposit more Fe, *etc*.

We have tried the first two methods here. Method 3 is relevant to lower temperature and will be tried in

the future. In each case, after cyclic deposition, the catalyst complex is reduced back to the active metallic state by a brief exposure to hydrogen, ammonia, or similar agent, depending on the oxygen affinity of the metal (Fe, Co, or Ni).[30] Nanotube growth is then carried out in a hydrogen-diluted acetylene.

Figure 2 shows the effectiveness of the process, using process conditions deliberately chosen to provide larger than usual nanoparticles that are more easily visible by atomic force microscopy (AFM). Figure 2a shows an AFM image of the catalyst nanoparticles before CNT growth after a single cycle of Fe deposition and anneal. The measured particle density is about 1.1×10^{10} cm^{-2}. Figure 2b shows the AFM image after two Fe deposition and anneal cycles. The measured particle density is now 1.8×10^{11} cm^{-2}. The average particle height increased only slightly from 9.6 to 10.2 nm. This suggests that the second nanoparticle layer fall into the dips *between* the first layer particles to minimize interfacial energy (insets of Figure 2). Figure 3 shows an AFM image of catalyst nanoparticles after two cycles of deposition and anneal of 0.3 nm of Fe films, with a final nanoparticle density estimated as 2.0×10^{13} cm^{-2}.

The area density of nanotubes can be measured in three ways. The first method is counting CNTs in a scan-
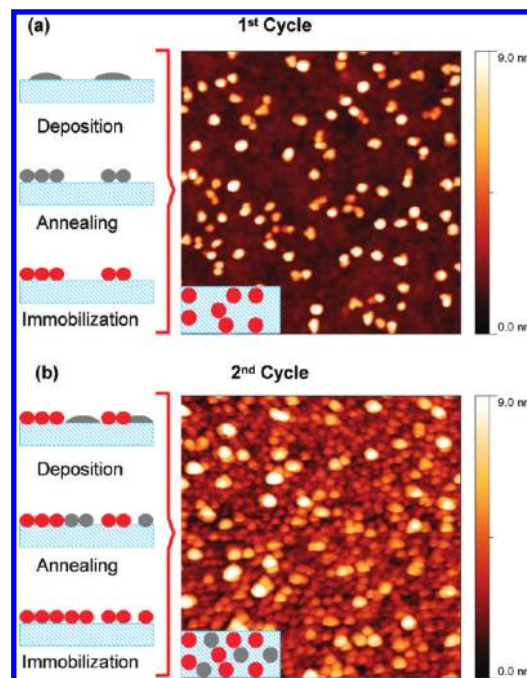

Figure 2. Catalyst design. The left-hand column shows schematically the standard (cycle 1) catalyst preparation method, and below, the additional cycle 2 steps of immobilization, deposition, and annealing. Cycle 2 can be repeated. The right-hand column shows AFM images of the catalyst nanoparticles after the standard and cyclic process, together with inset cartoons showing the particles deposited in cycles 1 and 2. A 0.5 nm Fe deposited onto Al_2O_3 after the first and second cycle of catalyst formation. Annealing is carried out in a furnace tube in ambient Ar/H$_2$ (1000:500 sccm) at 1 bar, from room temperature up to 750 °C at a heating rate of 75 °C min^{-1} for the first cycle and 25 °C min^{-1} for the second one.
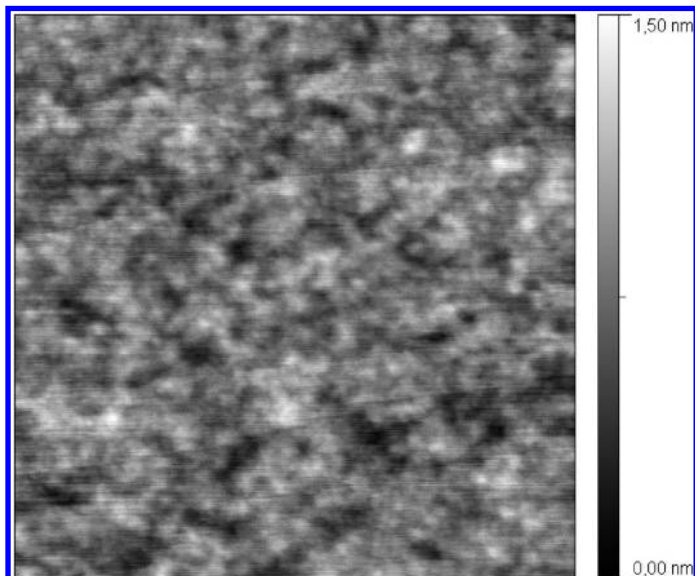
Figure 3. AFM scan of the catalyst nanoparticles after the cyclic deposition process, before nanotube growth.

ning electron microscopy (SEM) image or transmission electron microscopy (TEM) image. This method is less quantitative but gives an indication of higher density as the nanotubes become straighter at higher density as their confinement increases. The second method is weight gain. Supergrowth nanotubes are long enough that the area density can be derived from the sample weight gain during growth,[18] divided by the forest height, and divided by the nanotube mass per unit length, as calculated from its diameter and number of nanotube walls as measured by high-resolution (HR)TEM. The third method is liquid-induced compaction,[7,31] in which the forest is dipped into a liquid such as isopropyl alcohol and the wetting/drying process compacts the forest to a
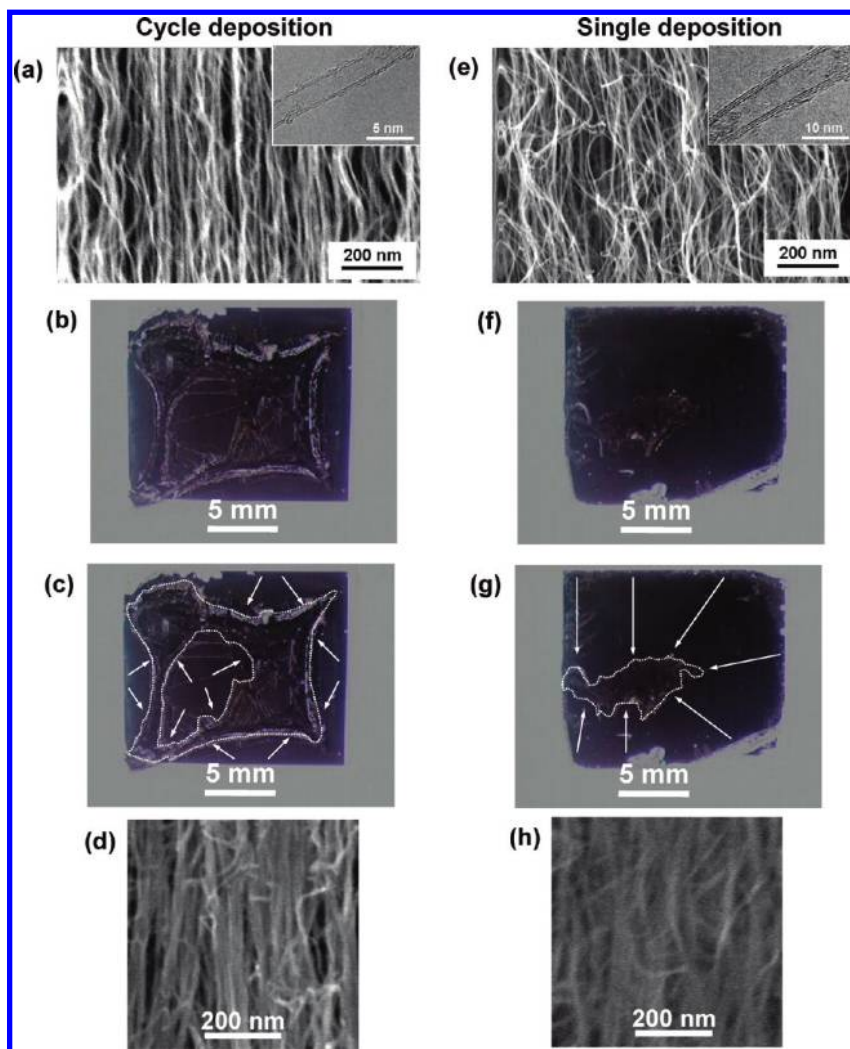

Figure 4. CNT growth and density measurement. (a,e) SEM and (inset) HRTEM images of CNTs grown for the 1 and 2 cycle processes. (b,f) Optical top view of the forests after liquid-induced compaction. (c,g) Illustration of extent of compacted regions. (d,h) Cross-sectional SEM images of the nanotubes in the compacted forests, showing straighter nanotubes in denser sample on left. The nanotubes were grown in a furnace tube using ambient $Ar/H_2/C_2H_2$ (1000:500:10 sccm) for 15 min at 750 °C and 1 bar. The catalyst is prepared using one or two cycles of 0.3 nm Fe onto Al_2O_3.
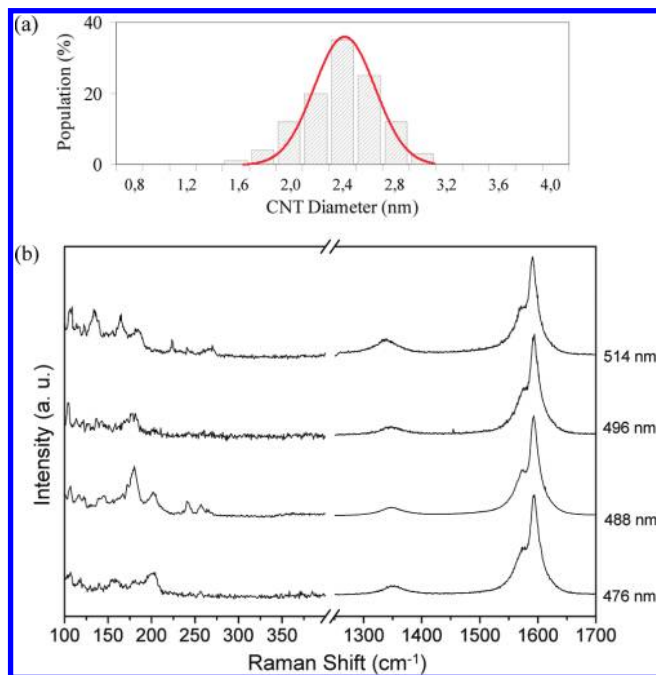
Figure 5. (a,b) Histogram showing diameter distribution with Gaussian fitting (red solid lines) and Raman spectra of nanotubes grown on two cycles of 0.3 nm Fe onto Al_2O_3.

maximum density. The area density is derived from the reduction in top surface area of patterned regions. We find that the latter two methods give quantitative and consistent values for the area density. It should be noted, however, that the compacted density does depend on the starting density. This is because the compacted density is higher for straighter CNT forests, as each crossover limits the compaction. We estimate a maximum compacted density of $\sim$1.58 g cm^{-3}, whereas Futaba[7] only achieved 0.95 g cm^{-3}, which is close to our *starting* density for our best case.

Figure 4 compares images of nanotube forests grown by the cyclic method (left) and the standard single cycle method (right). Figure 4a shows a cross-
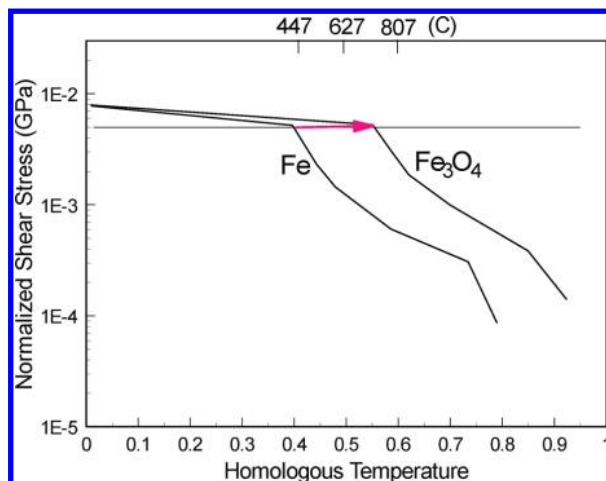

Figure 6. Deformation map for Fe and Fe_3O_4 for a strain rate of 10^{-3} s^{-1}, showing that a higher temperature is needed to deform the oxide.

section FEG (field emission gun) SEM side-view image of our ultrahigh density nanotube forest. The tubes are denser and much straighter than in forests of previously typical density, seen in Figure 4e. The HRTEM image (Figure 4a, inset) shows double-walled nanotubes (DWNTs). Figure 5a shows the diameter distribution with a mean diameter of 2.4 $\pm$ 0.2 nm. Raman gives a G/D peak ratio of 6 (Figure 5b). The measured mass density is 0.975 g cm^{-3}, giving an area density of 1.04 $\times$ 10^{13} cm^{-2}.

Figure 4b shows a top-view optical image of the forest after compaction. The central black area is nanotubes, the surrounding grayer area is the Si substrate where the forest was stripped off by lateral forces. Figure 4c shows schematically the top area of Figure 4b, while Figure 4d is the cross-section FEGSEM image of compacted forests, showing how very dense tubes bundle together. The liquid compaction method gives a filling factor of 62% for the two-cycle process and a density of 1 $\times$ 10^{13} cm^{-2}, similar to that by weight gain. Overall, a number of two-cycle samples were grown with heights of 180$-$300 μm, CNT diameters of 2.2$-$2.6 nm, mass density of 0.911 to 1.03 g cm^{-3}, pitch between nanotube centers of 3.1 to 3.4 nm, and resulting area densities of 0.92$-$1.10 $\times$ 10^{13} cm^{-2}.

The mass density of 0.975 g cm^{-3} of our uncompacted forest is a factor of 15 higher than the previous highest value of $\sim$0.06 g cm^{-3}.[7,18] This corresponds to a filling factor of 62% of the density 1.57 g cm^{-3}, the mass density of a fully dense DWNT forest of 2.4 nm diameter separated by the graphite interlayer spacing of 0.34 nm. For comparison, a fully dense forest of 1 nm diameter SWNTs has a mass density of 1.58 g cm^{-3}. The reference density is that of a fully dense mat, not that of graphite, as the atomic packing in nanotubes is lower than in graphite (density 2.515 g cm^{-3}).

For comparison, we deposited and annealed a single 0.6 nm Fe film (Figure 4, right). Figure 4e shows a cross-section FEGSEM image of the typical (lower) density nanotube forests. The CNTs are more bent in the low-density case due to less volume constraints. Figure 4f,g shows the typical forest after compaction, where the degree of compaction is much greater because its starting density is much lower. The density from the single-layer 0.6 nm case gives 1.34 $\times$ 10^{12} cm^{-2} with a mass density = 0.193 g cm^{-3}. Liquid compaction gives a filling factor of under 10%.

DISCUSSION

The key to immobilizing catalyst nanoparticles after each restructuring step is to convert them into a less deformable oxide or nitride before the next cycle. Consider Fe and Fe_3O_4. Restructuring Fe into nanoparticles is driven by surface energy minimization and occurs by plastic deformation/diffusion. The shear moduli, μ, of Fe and Fe_3O_4 or Fe_2O_3 are each $\sim$70 GPa, their melting temperatures are $\sim$1800 K and each enters a plastic

flow regime at normalized shear stress of $\sim$0.003μ.[32] The surface energy of Fe is 1.7 J m^{-2},[33] giving a 1.7 GPa shear stress for a 1 nm diameter droplet. This is well into the plastic flow regime. An anneal time of 10 min is equivalent to a strain rate of $\sim$10^{-3} s^{-1} for restructuring. The key difference between a metal and its oxide is that Fe has a strain rate of 10^{-3} s^{-1} at homologous temperature $\theta = 0.39$ or $T = 420$ °C, whereas Fe_3O_4 or Fe_2O_3 requires $\theta = 0.47$ or $T = 690$ °C (Figure 6) because of the slower diffusion rates of oxides. (For NiO or CoO, the range extends to 820 °C.) This gives a 270 °C window to restructure an upper Fe layer without affecting an underlying FeO_x layer.

Growth is presently carried out at 750 °C, a temperature higher than ideal in order to avoid deposition of amorphous carbon on CNT side walls, which would affect the weight gain values.[34] The Raman spectra (Figure 5b) showing a small D peak at 1350 cm^{-1} confirm the high purity of the tubes, with little amorphous carbon present. Generally, such deposition occurs after long exposure times,[35] whereas we used only a short growth period of 15 min. The D/G peak ratio is the same along the height of the forest. The forests have a similar area density at all heights, as we do not grow until growth termination, in which case the area density can fall due to, for example, catalyst sintering.[36] Our high density forests contain a random distribution of chiralities, as can be seen from the radial breathing modes in the Raman spectra of Figure 5b, as do the normal "supergrowth" forests.[37]

In summary, we demonstrate a catalyst design using cyclic deposition, annealing, and immobilization, which achieves an area density of 1.1×10^{13} cm^{-2}, 30 times greater than previously achieved. This allows carbon nanotubes to be used in microelectronics as vias and interconnects. Further optimization to the nanotube diameter to 1 nm and using more cycles will raise density to 10^{14} cm^{-2}, close to that of a fully dense forest. Our process requires no special equipment and is scalable to large areas, without scanning, unlike cluster beam methods.[38] It is also useful for heat spreaders, gecko films, supercapacitors, and NEMS.[8]

METHODS

We use as substrate polished Si(100), cut into pieces of $\sim$2 cm $\times$ $\sim$2 cm, covered with a layer of 200 nm of thermal SiO_2 and a topmost layer of 10 nm Al_2O_3. The catalyst films are deposited by thermal evaporation (without heating the substrate) of 0.1 to 0.5 nm nominal thickness high-purity Fe, Co, or Ni. The evaporation rate is <1 Å s^{-1} at <10^{-6} mbar base pressure, and the film thickness is monitored *in situ* by a quartz crystal microbalance and calibrated *ex situ* by atomic force microscopy (AFM) (Veeco Dimension) and spectroscopic ellipsometry. All samples are transferred in air and pretreated using a hot wall system (quartz furnace tube) at 500 to 750 °C in 1 bar Ar/H$_2$ (1000: 500 sccm) at heating rates between 12.5 and 75 °C min^{-1}. For annealing between cycles of catalyst deposition, the sample is removed from the furnace after reaching the final annealing temperature. Immediately after last annealing, the growth is carried out at the same temperature and pressure using Ar, H$_2$, and C$_2$H$_2$ (1000:500:10 sccm). After a growth period of 15 min, the samples are cooled in Ar.

The samples are characterized by field emission gun scanning electron microscopy (LEO 1530VP), AFM in tapping mode, high-resolution transmission electron microscopy (HRTEM) (FEI Tecnai F20, 200 kV), and Raman spectroscopy (476, 488, 496, and 514.5 nm excitation). Optical images are taken with a modular stereomicroscope (LEICA MZ 12.5) dotted with 12.5:1 zoom magnification changer and a digital camera. For HRTEM analysis, CNTs are removed from the substrates and dispersed onto carbon TEM grids. The nanoparticle density is derived from AFM images using ImageJ and Gwyydion software. The area density of nanotubes is calculated by the weight gain method. We measure the weight gain (AE ADAM analytical balance, resolution 10^{-4} g) per unit area of the sample and the height of the nanotube mat; we then correlate these values to the diameter and number of walls of the nanotubes, as determined by HRTEM. The TEM data give us the weight per nanotube unit length, so the nanotube density is given by the ratio of the sample weight gain to nanotube weight per unit length, which allows the mass per unit length to be calculated.

For compaction, we drip isopropyl alcohol, acetone, or ethyl alcohol onto the samples and allow them to dry out in clean room environment at 25 °C for 24 h. All experiments are systematically repeated to verify repeatability.

REFERENCES AND NOTES

1. Baughman, R. H.; Zakhidov, A. A.; de Heer, W. A. Carbon Nanotubes—The Route toward Applications. *Science* **2002**, *297*, 787–792.
2. Frank, S.; Poncharal, P.; Wang, Z. L.; de Heer, W. A. Carbon Nanotube Quantum Resistors. *Science* **1998**, *280*, 1744–1746.
3. Kim, P.; Shi, L.; Majumdar, A.; McEuen, P. L. Thermal Transport Measurements of Individual Multiwalled Nanotubes. *Phys. Rev. Lett.* **2001**, *87*, 215502–215505.
4. Kim, P.; Shi, L.; Majumdar, A.; McEuen, P. L. *Phys. Rev. Lett.* **2001**, *87*, 215502.
5. Dalton, A. B.; Collins, S.; Muñoz, E.; Razal, J. M.; Ebron, V. H.; Ferraris, J. P.; Coleman, J. N.; Kim, B. G.; Baughman, R. H. Super Tough Carbon Nanotube Fibres—Extraordinary Xomposite Fibres Can Be Woven Into Electronic Textiles. *Nature* **2003**, *423*, 703.
6. Simon, P.; Gogotsi, Y. Materials for Electrochemical Capacitors. *Nat. Mater.* **2008**, *7*, 845–854.
7. Futaba, D. N.; Hata, K.; Yamada, T.; Hiraoka, T.; Hayamizu, Y.; Kakudate, Y.; Tanaike, O.; Hatori, H.; Yumura, M.; Iijima, S. Shape-Engineerable and Highly-Dense Packed Single-Walled Carbon Nanotubes and Their Application as Super-Capacitor Electrodes. *Nat. Mater.* **2006**, *5*, 987–994.
8. Hayamizu, Y.; Yamada, T.; Mizuno, K.; Davis, R. C.; Futaba, D. N.; Yumura, N.; Hata, K. Integrated Three-Dimensional Microelectromechanical Devices from Processable Carbon Nanotube Wafers. *Nat. Nanotechnol.* **2008**, *3*, 289–294.
9. Hata, K.; Futaba, D. N.; Mizuno, K.; Namai, T.; Yumura, M.; Iijima, S. Water-Assisted Highly Efficient Synthesis of Impurity-Free Single-Walled Carbon Nanotubes. *Science* **2004**, *306*, 1362–1364.
10. Li, Y. L.; Kinloch, I. A.; Windle, A. H. Direct Spinning of Carbon Nanotube Fibers from Chemical Vapor Deposition Synthesis. *Science* **2004**, *304*, 276–278.
11. Li, X.; Cao, A.; Jung, Y. J.; Vijtai, R.; Ajayan, P. M. Bottom-Up Growth of Carbon Nanotube Multilayers, Unprecedented Growth. *Nano Lett.* **2005**, *5*, 1997–2000.
12. Cantoro, M.; Hofmann, S.; Pisana, S.; Scardaci, V.; Parvez, A.; Ducati, C.; Ferrari, A. C.; Blackburn, A. M.; Wang, K. Y.;

Robertson, J. Catalytic Chemical Vapor Deposition of Single-Wall Carbon Nanotubes at Low Temperatures. *Nano Lett.* **2006**, *6*, 1107–1112.

13. Harutyunyan, A. R.; Chen, G. A.; Paronyan, T. M.; Pigos, E. M.; Kuznetsov, O. A.; Hewaparakrama, K.; Kim, S. M.; Zakarov, D.; Stach, E. A.; Sumanasekera, G. U. Preferential Growth of Single Walled Carbon Nanotubes with Metallic Conductivity. *Science* **2009**, *326*, 116–120.

14. Wei, B. Q.; Vajtai, R.; Ajayan, P. M. Reliability and Current Carrying Capacity of Carbon Nanotubes. *Appl. Phys. Lett.* **2001**, *79*, 1172–1174.

15. Nihei, M.; Horibe, M.; Kawabata, A.; Awano, Y. Simultaneous Formation of Multiwall Carbon Nanotubes and Their End-Bonded Ohmic Contacts to Ti Electrodes for Future ULSI Interconnects. *Jpn. J. Appl. Phys.* **2004**, *43*, 1856–1859.

16. Yokoyama, D.; Iwasaki, T.; Ishimaru, K.; Sato, S.; Hyakushima, T.; Nihei, M.; Awano, Y.; Kawarada, H. Low Temperature Grown Carbon Nanotube Interconnects Using Inner Shells by Chemical Mechanical Polishing. *Appl. Phys. Lett.* **2007**, *91*, 263101–263103.

17. Futaba, D. N.; Hata, K.; Namai, T.; Yamada, T.; Mizuno, K.; Hayamizu, Y.; Yumura, M.; Iijima, S. 84% Catalyst Activity of Water-Assisted Growth of Single Walled Carbon Nanotube Forest Characterization by a Statistical and Macroscopic Approach. *J. Phys. Chem. B* **2006**, *110*, 8035–8038.

18. Zhong, G. F.; Iwasaki, T.; Kawarada, H. Semi-quantitative Study on the Fabrication of Densely Packed and Vertically Aligned Single-Walled Carbon Nanotubes. *Carbon* **2006**, *44*, 2009–2014.

19. Murakami, Y.; Chiashi, S.; Miyauchi, Y.; Hu, M.; Ogura, M.; Okubo, T.; Maruyama, S. Growth of Vertically Aligned Single-Walled Carbon Nanotube Films on Quartz Substrates and Their Optical Anisotropy. *Chem. Phys. Lett.* **2004**, *385*, 298–303.

20. Noda, S.; Hasegawa, K.; Sugime, H.; Kakehi, K.; Zhang, Z.; Maruyama, S.; Yamaguchi, Y. Millimeter-Thick Single-Walled Carbon Nanotube Forests. *Jpn. J. Appl. Phys.* **2007**, *46*, L399.

21. Yamazaki, Y.; Saluma, N.; Katagiri, M.; Suzuki, M.; Sakai, T.; Sato, S.; Nihei, M.; Awano, Y. Synthesis of a Closely Packed Carbon Nanotube Forest by a Multi-Step Growth Method Using Plasma-Based Chemical Vapor Deposition. *Appl. Phys. Exp.* **2010**, *3*, 55002–55004.

22. Hu, X. J.; Padilla, A. A.; Xu, J.; Fischer, T. S.; Goodson, K. E. 3-Omega Measurements of Vertically Oriented Carbon Nanotubes on Silicon. *J. Heat Transfer* **2006**, *128*, 1109–1113.

23. Akoshima, M.; Hata, K.; Futaba, D. N.; Mizuno, K.; Baba, T.; Yumura, M. Thermal Diffusivity of Single-Walled Carbon Nanotube Forest Measured by Laser Flash Method. *Jpn. J. Appl. Phys.* **2009**, *48*, 05EC07.

24. Danielson, D. T.; Sparacin, D. K.; Michel, J.; Kimerling, L. C. Surface-Energy-Driven Dewetting Theory of Silicon-on-Insulator Agglomeration. *J. Appl. Phys.* **2006**, *100*, 083507–083516.

25. Kim, D.; Giermann, A. L.; Thompson, C. V. Solid-State De-wetting of Patterned Thin Films. *Appl. Phys. Lett.* **2009**, *95*, 251903–251905.

26. Hofmann, S.; Cantoro, M.; Kleinsorge, B.; Casiraghi, C.; Parvez, A.; Robertson, J.; Ducati, C. Effects of Catalyst Film Thickness on Plasma-Enhanced Carbon Nanotube Growth. *J. Appl. Phys.* **2005**, *98*, 034308–034315.

27. Yamada, T.; Namai, T.; Hata, K.; Futaba, D. N.; Mizuno, K.; Fan, J.; Yudasaka, M.; Yumura, M.; Iijima, S. Size-Selective Growth of Double-Walled Carbon Nanotube Forests from Engineered Iron Catalysts. *Nat. Nanotechnol.* **2006**, *1*, 131–136.

28. Esconjauregui, S.; Bayer, B. C.; Fouquet, M.; Wirth, C. T.; Ducati, C.; Hofmann, S.; Robertson, J. Growth of High-Density Vertically Aligned Arrays of Carbon Nanotubes by Plasma-Assisted Catalyst Pretreatment. *Appl. Phys. Lett.* **2009**, *95*, 173115–173117.

29. Cantoro, M.; Hofmann, S.; Mattevi, C.; Pisana, S.; Parvez, A.; Fasoli, A.; Ducati, C.; Scardaco, V.; Ferrari, A. C.; Robertson, J. Plasma Restructuring of Catalysts for Chemical Vapour Deposition of Carbon Nanotubes. *J. Appl. Phys.* **2009**, *105*, 064304.

30. Mattevi, C.; Wirth, C. T.; Hofmann, S.; Blume, R.; Cantoro, M.; Ducati, C.; Cepek, C.; Knop-Gericke, A.; Milne, S.; Castellarin-Cudia, C. In-Situ X-ray Photoelectron Spectroscopy Study of Catalyst-Support Interactions and Growth of Carbon Nanotube Forests. *J. Phys. Chem. C* **2008**, *112*, 12207–12213.

31. Chakrapani, N.; Wei, B.; Carrillo, A.; Ajayan, P. M.; Kane, R. S. Capillarity-Driven Assembly of Two-Dimensional Cellular Carbon Nanotube Foams. *Proc. Natl. Acad. Sci. U.S.A.* **2004**, *101*, 4009–4012.

32. Frost, H. J.; Ashby, M. F. *Deformation Maps*; Pergamon Press: Oxford, 1982.

33. Vitos, L.; Ruban, A. V.; Skriver, H. L.; Kollár, J. The Surface Energy of Metals. *Surf. Sci.* **1998**, *411*, 186–202.

34. Yasuda, S.; Hiraoka, T.; Futaba, D. N.; Yamada, T.; Yumura, M.; Hata, K. Existence and Kinetics of Graphitic Carbonaceous Impurities in Carbon Nanotube Forests To Assess the Absolute Purity. *Nano Lett.* **2009**, *9*, 769–773.

35. Zhong, G.; Iwasaki, T.; Robertson, J.; Kawarada, H. Growth Kinetics of 0.5 cm Long Vertically Aligned Single Walled Carbon Nanotubes. *J. Phys. Chem. B* **2007**, *111*, 1907.

36. Amama, P. B.; Pint, C. L.; McJilton, L.; Kim, S. M.; Stach, E. A.; Murray, T.; Hauge, R. H.; Maruyama, B. Role of Water in Super Growth of Single Walled Carbon Nanotubes. *Nano Lett.* **2009**, *9*, 44–49.

37. Robertson, J.; Zhong, G.; Telg, H.; Thomsen, C.; Warner, J. H.; Briggs, G. A. D.; Detlaff, U.; Roth, S. Growth and Characterization of High-Density Mats of Single-Wall Carbon Nanotubes for Interconnects. *Appl. Phys. Lett.* **2008**, *93*, 163111.

38. Kondo, D.; Sato, S.; Awano, Y. Low-Temperature Synthesis of Single-Walled Carbon Nanotubes with a Narrow Diameter Distribution Using Size-Classified Catalyst Nanoparticles. *Chem. Phys. Lett.* **2006**, *422*, 481–487.

ARTICLE